

Open camera or QR reader and  
scan code to access this article  
and other resources online.



**ORIGINAL ARTICLE**

# An Infection Model for SARS-CoV-2 Using Rat Transplanted with hiPSC-Airway Epithelial Cells

Masayuki Kitano, MD,<sup>1</sup> Hiroe Ohnishi, PhD,<sup>1</sup> Akiko Makino, PhD,<sup>2</sup> Tatsuo Miyamoto, PhD,<sup>3</sup>  
Yasuyuki Hayashi, MD, PhD,<sup>1</sup> Keisuke Mizuno, MD,<sup>1</sup> Shinji Kaba, MD, PhD,<sup>1</sup> Yoshitaka Kawai, MD, PhD,<sup>1</sup>  
Tsuyoshi Kojima, MD, PhD,<sup>1</sup> Yo Kishimoto, MD, PhD,<sup>1</sup> Norio Yamamoto, MD, PhD,<sup>1,4</sup> Keizo Tomonaga, PhD,<sup>2</sup> and  
Koichi Omori, MD, PhD<sup>1</sup>

Investigating the infection mechanism of severe acute respiratory syndrome coronavirus 2 (SARS-CoV-2) in the airway epithelium and developing effective defense strategies against infection are important. To achieve this, establishing appropriate infection models is crucial. Therefore, various *in vitro* models, such as cell lines and primary cultures, and *in vivo* models involving animals that exhibit SARS-CoV-2 infection and genetically humanized animals have been used as animal models. However, no animal model has been established that allows infection experiments with human cells under the physiological environment of airway epithelia. Therefore, we aimed to establish a novel animal model that enables infection experiments using human cells. Human induced pluripotent stem cell-derived airway epithelial cell-transplanted nude rats (hiPSC-AEC rats) were used, and infection studies were performed by spraying lentiviral pseudoviruses containing SARS-CoV-2 spike protein and the *GFP* gene on the tracheae. After infection, immunohistochemical analyses revealed the existence of GFP-positive-infected transplanted cells in the epithelial and submucosal layers. In this study, a SARS-CoV-2 infection animal model including human cells was established mimicking infection through respiration, and we demonstrated that the hiPSC-AEC rat could be used as an animal model for basic research and the development of therapeutic methods for human-specific respiratory infectious diseases.

**Keywords:** hiPSC, trachea, transplantation, infection model, artificial trachea

## Impact Statement

Infection models are important to elucidate the mechanism of infection and to develop defense or therapeutic methods against infection; however, no research model permitting infection experiments with human cells under the physiological environment of airway epithelial tissue has been established. Therefore, we aimed to establish a novel infection model mimicking infection through respiration using human cells, performed infection experiments by spraying pseudovirus into hiPSC-AEC rats, and confirmed infection in human cells. This infection model could serve as an animal model for basic research and the development of therapeutic methods for human-specific respiratory infectious diseases.

<sup>1</sup>Department of Otolaryngology–Head and Neck Surgery, Graduate School of medicine, Kyoto University, Kyoto City, Japan.

<sup>2</sup>Department of Virus Research, Institute for Life and Medical Sciences, Kyoto University, Kyoto City, Japan.

<sup>3</sup>Department of Molecular and Cellular Physiology, Research Institute for Cell Design Medical Science, Graduate School of Medicine, Yamaguchi University, Ube City, Japan.

<sup>4</sup>Department of Otolaryngology, Kobe City Medical Center General Hospital, Kobe city, Japan.

## Introduction

The coronavirus disease 2019 (COVID-19) pandemic was caused by severe acute respiratory syndrome coronavirus 2 (SARS-CoV-2).<sup>1,2</sup> SARS-CoV-2 belongs to the *Betacoronavirus* genus, the same as SARS-CoV and middle East respiratory syndrome coronavirus, which have repeatedly caused international outbreaks,<sup>3</sup> and infection with these viruses typically begin in the upper respiratory tract and spreads to the lower respiratory tract and other organs.<sup>4–6</sup> During infection in humans, multiciliated cells in the nasopharynx or trachea are likely to be the first cells targeted by SARS-CoV-2, in parallel with sustentacular cells in the nasal olfactory mucosa.<sup>7</sup> Several SARS-CoV-2 variants emerged during the COVID-19 pandemic. The target tissue of infection and primary symptoms vary among the variants. For example, being significantly different from previous variants, the Omicron variant causes infection mainly to the upper respiratory tract and lower respiratory tract infections less frequently.<sup>5,8</sup>

SARS-CoV-2 is composed of structural proteins, nucleocapsid, membrane, envelope, and spike (S) proteins, and the S protein serves as the infectious ligand. The S proteins form homotrimers and are inserted into the virus membrane in multiple copies. The S protein consists of S1 and S2 subunits. S1 binds to the angiotensin-converting enzyme 2 (ACE2) receptor, and S2 fuses the virus to the host cell membrane. The RNA and viral proteins of SARS-CoV-2 are transferred to host cells through the fusion pore formed via membrane fusion. Host proteins other than ACE2 that function as receptors have been identified,<sup>9</sup> and details of infection mechanisms are expected to emerge in the future.

Infection models are necessary to elucidate such infection mechanisms and develop therapeutic agents.<sup>10</sup> It is important to elucidate the mechanism of infection in the airway epithelium as the first targeted site and develop methods of defense against infection. However, no research models allowing infection experiments with human cells under the physiological environment of airway epithelial tissue are available. In the early stages of the epidemic, cell lines were mainly used as *in vitro* models.<sup>11–14</sup> Subsequently, primary cultures of human airway cells<sup>15</sup> and human-induced pluripotent stem cell (hiPSC)-derived cells including organoids<sup>16–19</sup> were used for further studies as infection models closer to the human body. Hamsters and nonhuman primates, which exhibit SARS-CoV-2 infection, have been used as animal models, and genetically humanized animals, in which genes involved in infection are replaced with human sequences, have also been used.<sup>20,21</sup> Although the interaction of SARS-CoV-2 and ACE2 can be studied using transgenic mice expressing human ACE2, it is unlikely that they fully reproduce the pathological conditions in humans because other genes are of mouse origin.

As an animal model using human cells, a humanized mouse model in which a human fetal lung was transplanted subcutaneously was reported.<sup>22,23</sup> However, this mouse model did not reproduce infection from inhalation because infection experiments in that study were performed by injecting the virus into the subcutaneous graft directly. We have already established a “hiPSC-AEC rat” in which hiPSC-derived airway epithelial cells (hiPSC-AECs) were transplanted into the tracheae of

immunodeficient rats.<sup>24</sup> Therefore, these hiPSC-AEC rats can permit SARS-CoV-2 infection experiments through the physiological infection route.

In this background, we aimed to establish a novel infection model using human cells, performed infection experiments using hiPSC-AEC rats that were sprayed with pseudovirus, and investigated infection in human cells by histological analysis.

## Materials and Methods

### Virus

As infection studies using SARS-CoV-2 require biosafety level (BSL)-3 facilities, we used a nonreplicative pseudovirus containing the S protein of SARS-CoV-2, which can be used in BSL-2 laboratories. SARS-CoV-2 pseudovirus (lenti-virus backbone pseudovirus, with S protein of SARS-CoV-2 [B.1.1.529, Omicron], which expresses EGFP after infection) was purchased from VectorBuilder Japan.

### Cell lines

HEK293T cells and the hiPSC 253G1 cell line were obtained from RIKEN BioResource Research Center. HEK293T cells were maintained in Dulbecco's modified Eagle's medium (DMEM, Nacalai Tesque) containing 100 U/mL penicillin, 100 µg/mL streptomycin solution, and 10% fetal bovine serum (COSMO BIO). HiPSCs were maintained in the feeder-free system using Essential 8 Medium (ThermoFisher Scientific) on a Geltrex (ThermoFisher Scientific)-coated culture plate for 10 passages before induction.

### Generation of HEK293T cells expressing human ACE2

To generate HEK293T cells stably expressing human ACE2 and mCherry fusion protein (hACE2-mCherry/HEK293T cells), the pX330 plasmid containing sgRNA (5'-GGGGCCACTAGG-GACAGGAT-3') and Cas9, and the targeting plasmid vector consisting of human *ACE2*, *mCherry*, T2A sequence, puromycin *N*-acetyl-transferase, and a CMV promoter-driven hsvTK-2A-Neo cassette<sup>25</sup> in the pBlueScript II SK (-) backbone, were used. Two types of plasmid vectors were cotransfected into HEK293T cells using Lipofectamine™ 2000 Transfection Reagent (ThermoFisher Scientific). After 2 days, the cells were reseeded and selected with 0.5 µg/mL puromycin (Fujifilm Wako). Each clone was selected by fluorescence of mCherry, and the selected clone was expanded and used for the subsequent study.

### Induction of AECs from hiPSCs (hiPSC-AECs)

AECs were induced from hiPSCs according to the method described previously.<sup>26,27</sup> HiPSCs were seeded on Geltrex-coated plates in the basal medium consisting of RPMI1640 medium (Nacalai Tesque), 1 × B27 supplement (ThermoFisher Scientific), and 50 U/mL penicillin/50 µg/mL streptomycin, 100 ng/mL supplemented with human activin A (R&D System), 1 µM CHIR99021 (Axon Medchem), and 10 µM Y-27632 (day 0), 0.25 mM (day 1), or 0.125 mM (days 2–4) sodium butyrate (Wako) for differentiation of cells into endoderm. From days 6 to 28, the medium consisting of DMEM/F-12 with GlutaMAX (Life Technologies), 1 × B27 supplement, 50 U/mL penicillin/streptomycin, 0.05 mg/mL L-ascorbic

acid (Wako), and 0.4 mM monothioglycerol (FUJIFILM Wako) was used as the basal medium. From days 6 to 9, cells were cultured in basal medium supplemented with 100 ng/mL human recombinant noggin (Human Zyme) and 10  $\mu$ M SB431542 (Stem RD) (step 2). Then, the cells were cultured in basal medium supplemented with 20 ng/mL human recombinant BMP4 (Human Zyme), 2.5  $\mu$ M CHIR99021, and 0.1  $\mu$ M all-trans retinoic acid (Sigma-Aldrich). On day 14, objective cells were purified by magnetic-activated cell sorting using an anti-carboxypeptidase M (CPM) antibody (FUJIFILM Wako), which is a surface marker of NKX2-1-positive ventralized anterior foregut endoderm cells.<sup>26</sup> CPM-positive cells were suspended with the mixture of basal medium supplemented with 3.0  $\mu$ M CHIR99021, 100 ng/mL FGF10 (FUJIFILM Wako), 10  $\mu$ M Y27632, and growth factor-reduced Matrigel at a ratio of 1:1. Cells were embedded and maintained on 12-well cell culture inserts with polyethylene terephthalate membrane (Corning, #353292) for 14 days (days 14–27). On day 28, the medium was changed to the step 5 medium consisting of PneumaCult-ALI Maintenance medium (STEMCELL Technologies), 10  $\mu$ M Y 27632, 4  $\mu$ g/mL heparin (Nacalai Tesque), 1  $\mu$ M hydrocortisone (Sigma-Aldrich), and 10  $\mu$ M DAPT (FUJIFILM Wako). On day 42, a single-cell suspension was obtained from the spheroids by enzymatic treatment and seeded on 12-well cell culture inserts with collagen vitrigel membrane (ad-MED Vitrigel 2, Kanto Chemical Co.). For 14 days, the cells were cultured in the step 5 medium under the air–liquid interface condition to lead the AEC layer, and this collagen vitrigel membrane with the hiPSC-AECs on it was used for the infection assay and transplantation as cell sheets.

#### Electron microscopy

Induced cells on the vitrigel membranes were fixed with 4% paraformaldehyde (PFA) and 2% glutaraldehyde/phosphate-buffered saline (PBS) overnight at 4°C, incubated in 1% osmium tetroxide (Nacalai Tesque) for 2 h, and dehydrated using ascending ethanol concentrations. For scanning electron microscopy (SEM), dehydrated cells were dried using the critical point drying method and coated with platinum palladium. For transmission electron microscopy (TEM), dehydrated cells were embedded in epoxy resin and DMP-30 (Nacalai Tesque) and sectioned. The specimens were observed under an SEM (S-4700; Hitachi Co.) or a TEM (H7650; Hitachi).

#### Preparation of artificial tracheae

The collagen solution (6 mg/mL, Nippon Meat Packers, Inc.) was adjusted to pH 7.0 and centrifuged. Then, the collagen pellet was frozen at –80°C and lyophilized for 10 days. The dried collagen was then cut into small pieces, dissolved in ultrapure water (106.4 mg/mL) while hydrochloric acid was added, and adjusted to pH 3. The collagen solution was poured into a mold, a polypropylene mesh coated with the collagen solution was added, an equal volume of the collagen solution was poured, and then it was frozen at –80°C overnight. After 1 week of lyophilization, collagen, including polypropylene mesh, was cross-linked by heating, sterilized by ethylene oxide gas, and stored in a desiccator.

#### Pseudovirus infection assay *in vitro*

For the infection assay using HEK293T, the mixture of HEK293T and hACE2-mCherry/HEK293T cells was seeded at a split ratio of 2:1 on the 96-well culture plates coated with  $\epsilon$ -poly-L-lysine (COSMO BIO) at a concentration of  $1 \times 10^4$  cells/well. After 2 days, the medium was replaced with 100  $\mu$ L of the maintenance medium containing  $1 \times 10^7$  TU/mL pseudovirus and 2  $\mu$ g/mL polybrene. On the next day, the medium was replaced with a maintenance medium and cultured for 3 days. For the infection assay using hiPSC-AECs, the medium in the culture insert was replaced with 100  $\mu$ L of the step 5 medium containing  $5 \times 10^8$  TU/mL pseudovirus and 2  $\mu$ g/mL polybrene. On the next day, the medium inside and outside the culture insert was replaced with the step 5 medium, and cells were cultured for 7 days. After the infection assay, cells were fixed for the immunofluorescence analyses.

#### Animals

Male F344/NJcl-rnu/rnu nude rats, purchased from CLEA Japan, were used. The rats were 10–14 weeks old and weighed 200–320 g. The animal experimental protocol for this study was approved by the Animal Experimentation Committee of Kyoto University (Med Kyo 23116). All animal experiments in this study are performed according to the Guidelines for Animal Experiments of Kyoto University. The transplantation experiment and pseudovirus infection assay in the hiPSC-AEC rats were performed under anesthesia, with an intraperitoneal injection of midazolam (2 mg/kg), butorphanol tartrate (2.5 mg/kg), and medetomidine hydrochloride (0.15 mg/kg).

#### Transplantation

A total of 11 nude rats were used. The trachea was exposed by a midline neck skin incision and separation of the bilateral sternohyoid and sternothyroid muscles. A square tracheal defect was created by incision with a scalpel. The defect size was two tracheal rings (~2.5 mm) in length and 2 mm in width. An artificial trachea covered with a cell sheet was placed over the tracheal defect with the cells facing the tracheal lumen. Then, the cephalocaudal side of the graft was sutured to the trachea with 9-0 nylon sutures (BEAR medic). These rats were used as hiPSC-AEC rats.

#### Pseudovirus infection assay *in hiPSC-AEC rats*

Pseudovirus infection assays in hiPSC-AEC rats were performed 14 days after the transplantation. For tracheal injection, a 16-G intubation tube (KN-1007-1, Natsume Seisakusho) was intubated into the trachea using a guide wire (KN-1007-X1, Natsume Seisakusho). Then, 19-gauge intratracheal spray (KN-34700-4, Natsume Seisakusho) was inserted into the intubation tube (Supplementary Fig. S1). HiPSC-AEC rats were sprayed with 100  $\mu$ L of Hanks' Balanced Salt Solution (HBSS) (+) (Nacalai Tesque) containing 2  $\mu$ g/mL polybrene (control group, C1 – 5,  $n = 5$ ) or HBSS (+) containing  $1 \times 10^9$  TU/mL pseudovirus and 2  $\mu$ g/mL polybrene (pseudovirus infection group, V1 – 6,  $n = 6$ ) at the transplantation site in the

trachea. On day 7, after euthanasia, the tracheae including the transplantation site were collected for histological examination.

#### Immunofluorescence staining

After fixation with 4% PFA for 15 min, cells were permeabilized with 0.2% Triton X-100 for 5 min and treated with 1% bovine serum albumin (BSA; Wako) for 10 min at room temperature. Cells were incubated in primary antibodies overnight at 4°C, washed three times with PBS, and incubated with Alexa Fluor-conjugated secondary antibodies (ThermoFisher Scientific), Alexa Fluor 647-conjugate phalloidin (Santa Cruz), and 4',6-diamidino-2-phenylindole (DAPI) for 1 h at room temperature. The samples were mounted with Fluoromount-G Anti-Fade (SouthernBiotech). Images were captured using an Eclipse Ti-S fluorescence microscope (Nikon Corporation) equipped with a DP73 camera (Olympus) and a BX 50 fluorescence microscope equipped with a DP70 camera (Olympus).

After the infection experiments, the tracheae including grafts were fixed with 4% PFA for 24 h. Subsequently, tissues were immersed in 10%, 20%, and 30% sucrose for 24 h each and embedded in the Tissue-Tec optimal cutting temperature compound (Sakura Finetek Japan). Embedded tissues were sectioned at 10 µm thickness using a cryostat (CryoStar NX70, ThermoFisher Scientific), and sections at 100 µm intervals were used to calculate the survival rates of the transplanted cells, and sections at 30 µm intervals were used to calculate the number of infected cells. After washing with PBS, tissue sections were treated with 0.1% Triton X-100, 1% BSA, and 10% donkey serum in PBS for 30 min at room temperature. Then, sections were treated with primary antibodies (Table 1) overnight at 4°C and washed with PBS. Sections were treated with Alexa Fluor secondary antibodies (ThermoFisher Scientific), Alexa Fluor 647-conjugate phalloidin (Santa Cruz), and DAPI for 1 h at room temperature. Sections were mounted using Fluoromount-G Anti-Fade (SouthernBiotech) and observed using a BZ-X810 fluorescence microscope (Keyence).

For immunofluorescence staining, the following first antibodies were used: anti-FOXA2 antibody (R&D Systems, AF2400, 1:500), anti-NKX2.1 antibody (ThermoFisher Scientific, MS-699-P, 1:500), antiacetylated  $\alpha$ -tubulin (Ac-TUB) antibody (Sigma-Aldrich, T7451, 1:1000), anti-E-cadherin monoclonal antibody (ThermoFisher Scientific,

13-1900, 1:000), antihuman nuclei antigen (HNA) antibody (Millipore, MAB1281, 1:000), and GFP polyclonal antibody (Invitrogen, A-11122, 1:2000).

#### Quantification

Pseudovirus infection assays using HEK293T cells and hiPSC-AECs were performed three times each, and the proportions of GFP-positive cells in hACE2-mCherry/HEK293T cells, or hiPSC-AECs, from three independent 250 µm × 250 µm square areas, per experiment, were calculated as infection rates. To calculate the survival rate of the transplanted cells, two 350 µm wide areas in the center and one side of the transplanted area were analyzed. The proportion of HNA-positive cells in the epithelia was calculated as the survival rate of the transplanted cells. Moreover, the proportion of GFP, HNA, and GFP antibody-labeled triple-positive cells in the epithelia was calculated as the infection rate of the transplanted cells. Moreover, the number of GFP, HNA, and GFP antibody-labeled triple-positive cells in the epithelia of all transplanted areas was counted as the infected hiPSC-derived cells.

#### Statistical analysis

Statistical analyses were performed using EZR (Saitama Medical Center, Jichi Medical University), which is a graphical user interface for R (The R Foundation for Statistical Computing, Vienna, Austria) for Windows.<sup>28</sup> Data are expressed as medians (range; minimum—maximum value) or means ± standard deviations. The Mann–Whitney *U* test was used to compare two groups with independent samples. In all analyses,  $p < 0.05$  was considered statistically significant.

## Results

### Characterization of hiPSC-AECs

HiPSC-AEC induction was conducted (Fig. 1A) according to previous reports.<sup>26,27</sup> The expression of marker proteins in induced cells in each induction step was evaluated by immunohistochemical analyses. In the induced cells, expression of the endoderm marker FOXA2 (Fig. 1Ba) and ventralized anterior foregut endoderm cell marker NKX2-1 (Fig. 1Bb) was observed on days 6 and 14, respectively. On day 28, spheroid formation was confirmed in Matrigel by phase-contrast microscopy (Fig. 1Bc).

On day 56, in the surface observation of cells following hiPSC-AEC induction, multiciliated cells with Ac-TUB-positive cilia-like protrusions, which are likely to be the first target cells by SARS-CoV-2, were confirmed in E-cadherin-positive epithelial sheet (Fig. 1Bd). Furthermore, cilia-like protrusions were observed by SEM (Fig. 1Be) and TEM (Fig. 1Bf). The 9 + 2 microtubule arrangements, which are specifically observed in motile cilia, were confirmed in the cross-section of the cilia (Fig. 1Bf, inset).

### Pseudovirus infection assay *in vitro*

Infection assays using cell line cells were performed before the infection assay using hiPSC-AEC rats (Fig. 2A). To confirm whether the pseudovirus infection occurs depending on hACE2 expression, the mixture of HEK293T cells and hACE2-mCherry/HEK293T cells was infected

TABLE 1. SURVIVAL RATE OF hiPSC-AECs

Rat no.	Survival rate (%)
V-1	1.70
V-2	3.51
V-3	6.10
V-4	0.89
V-5	0.69
V-6	0.86
C-1	18.09
C-2	2.80
C-3	0.86
C-4	3.00
C-5	0.87

hiPSC-AECs, human-induced pluripotent stem cell-derived airway epithelia cells.

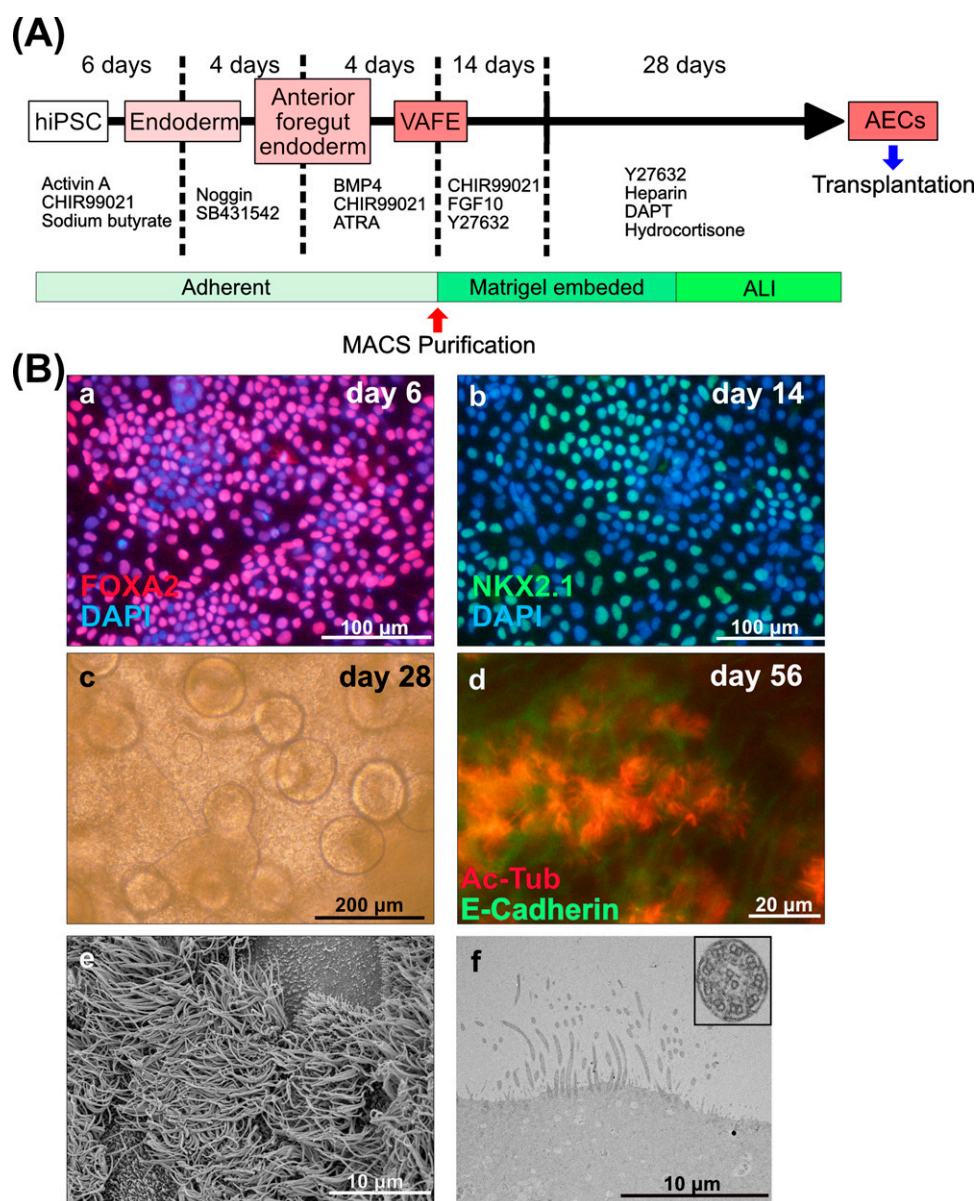


**FIG. 1.** Characterization of hiPSC-AECs. **(A)** Schema of hiPSC-AEC induction process. **(B)** Characterization of induced cells in each induction step in hiPSC-AEC induction. Immunofluorescence analyses of induced cells showed the expression of FOXA2 at day 6 **(a)**, NKX2-1 at day 14 **(b)**, and acetylated  $\alpha$ -tubulin and E-cadherin at day 56 **(d)**. At day 28, sphere formation in Matrigel was observed **(c)**. Scale bars: 100  $\mu$ m **(a)**, 100  $\mu$ m **(b)**, 200  $\mu$ m **(c)**, and 20  $\mu$ m **(d)**. Images of scanning electron microscope **(e)** and transmission electron microscope **(f)** showed cilia-like protrusions at the apical surface of hiPSC-derived AECs. Scale bars = 10  $\mu$ m. A 9 + 2 microtubule arrangement specific to motile cilia (*inset*) was shown in the cross section of the cilia. Ac-TUB, acetylated  $\alpha$ -tubulin; ALI, air-liquid interface; DAPI, 4',6-diamidino-2-phenylindole; hiPSC-AECs, human-induced pluripotent stem cell-derived airway epithelia cells; MACS, magnetic activated cell sorting; VAFE, ventralized anterior foregut endoderm cells.

with lentiviral pseudoviruses containing SARS-CoV-2S proteins and the *GFP* gene. Three days after infection, GFP-positive infected cells (Fig. 2Ba) were observed only in mCherry-positive HEK293T cells, which suggests ACE2 expression (Fig. 2Bb) in DAPI-positive cells (Fig. 2Bc). The infection rate (proportion of GFP-positive cells in total mCherry-positive HEK293T cells) was  $7.31\% \pm 1.75\%$ . This result indicates that pseudovirus infection occurs depending on hACE2 expression (Fig. 2Bd). Infection assays were also performed using HEK293T cells and

hACE2-mCherry/HEK293T cell separately. After infection, many GFP-positive infected cells were observed in hACE2-mCherry/HEK293T cell assays. In contrast, a few GFP-positive cells in HEK293T cells were considered to be accidental intake of pseudovirus through endocytosis (Supplementary Fig. S2). Then, pseudovirus infection experiments were conducted with hiPSC-AECs. hiPSC-AECs were infected with lentiviral pseudoviruses containing SARS-CoV-2S proteins and the *GFP* gene from the apical side. Seven days after infection, GFP-positive infected

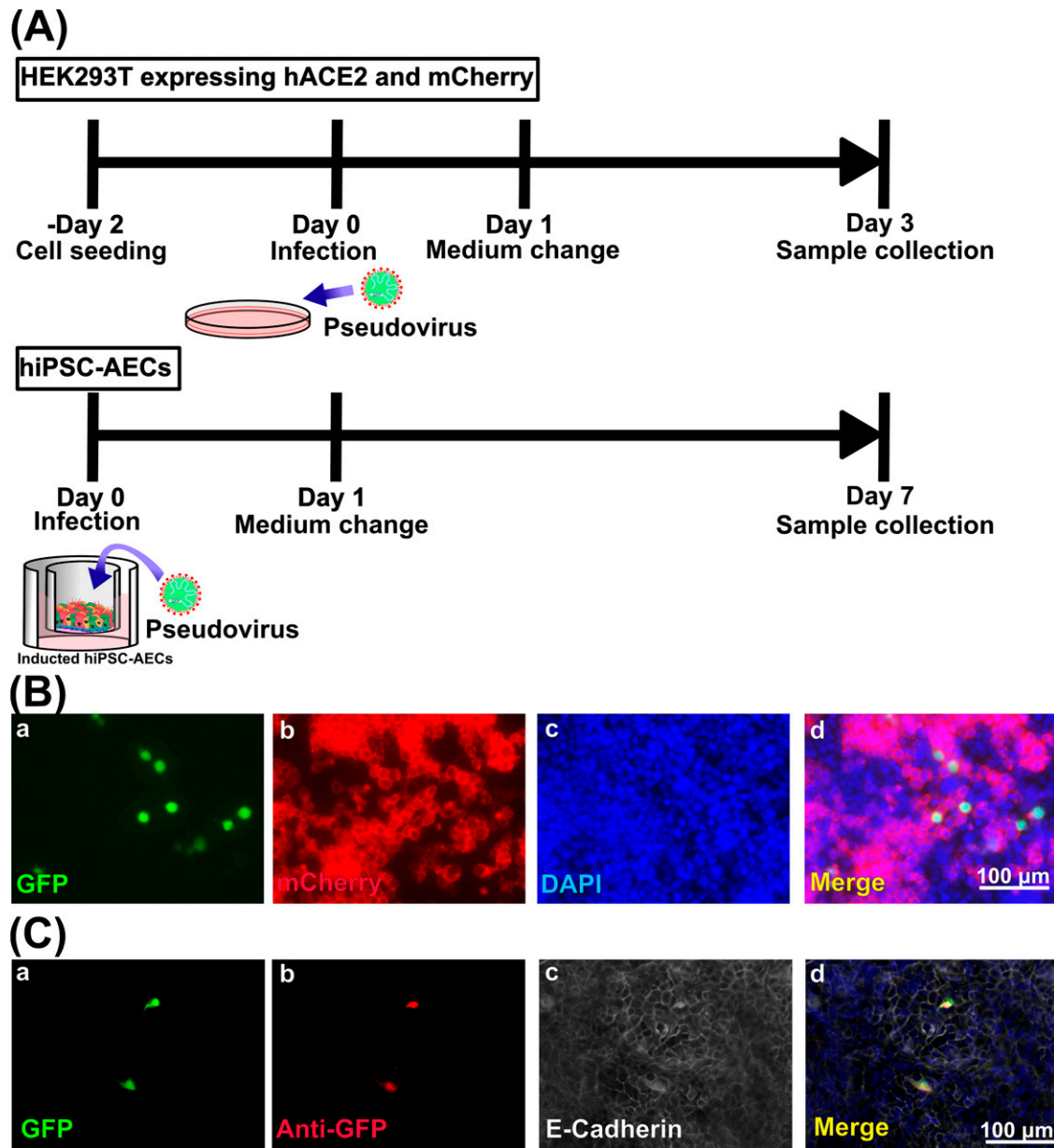


**FIG. 2.** Pseudovirus infection assay *in vitro*. **(A)** Timelines of *in vitro* infection assay. **(B)** Images of mixed culture of HEK293T cells and hACE2-mCherry/HEK293T cells after infection with lentiviral pseudoviruses containing SARS-CoV-2 spike proteins and the *GFP* gene. Infected cells expressing GFP **(a)** were observed in only mCherry-positive HEK293T cells and **(b)** in all DAPI-labeled HEK293T cells **(c)**. A merged image is shown in **(d)**. Scale bars = 100  $\mu$ m. **(C)** Images of hiPSC-AECs after infection with lentiviral pseudoviruses containing SARS-CoV-2 spike proteins and the *GFP* gene. Infected cells expressing GFP **(a)** and labeled with an anti-GFP antibody **(b)** were observed in E-cadherin-positive hiPSC-AEC sheet **(c)**. A merged image is shown in **(d)**. Scale bars = 100  $\mu$ m. hACE2, human angiotensin-converting enzyme 2.

cells (Fig. 2Ca, b) were observed in hiPSC-AECs (Fig. 2Cc, d). The infection rate (proportion of GFP-positive cells in total hiPSC-AECs) was  $0.78 \pm 0.45\%$ .

#### Generation of hiPSC-AEC rats

In this study, nude rats that were transplanted with grafts consisting of the artificial tracheae covered with hiPSC-AEC sheets were used as hiPSC-AEC rats (Fig. 3A). HiPSC-AEC rats were used for the infection assay on day 14 after transplantation. Six hiPSC-AEC rats used for pseudovirus infection

were randomly selected, and the remaining five HiPSC-AEC rats were sprayed with PBS instead of pseudoviruses to use as the control group. The tracheae including the transplanted areas were collected and used for the evaluation of survival and infection rates (Fig. 3B). The immunohistochemical images of the vertical sections of the transplanted areas (Fig. 4A) were used to calculate the survival rate of transplanted cells in the epithelia of the transplanted area (Fig. 4Ba). HNA-positive surviving hiPSC-AECs and hiPSC-derived cells (Fig. 4Bb) were observed in the transplanted area (Fig. 4Bc) (Table 1). The median survival rate of hiPSC-AECs in hiPSC-AEC

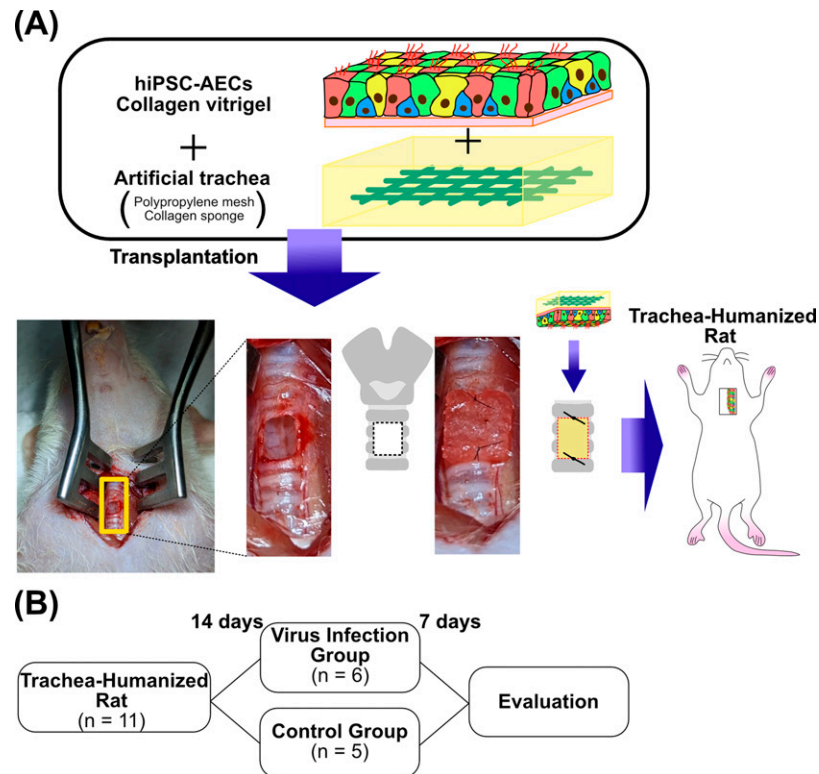


**FIG. 3.** Scheme of the experimental design of this study. **(A)** Scheme for the generation of hiPSC-AEC rats. Artificial tracheae covered with hiPSC-AECs on collagen vitrigel are transplanted into the nude rat tracheae. The graft was placed on the tracheal defect, with the cells facing the tracheal lumen. **(B)** Flowchart of the infection experiment. Two weeks after hiPSC-AEC rats generation, an infection study was conducted. One week after infection, tracheae including hiPSC-AECs were harvested for evaluation.

rats was 1.70% (0.69–18.08%). No statistical significance was observed in the survival rates of surviving transplanted cells in the epithelia of the transplanted area between two groups (virus infection group, 1.29% [0.68–6.10%]; control group, 2.80% [0.86–18.08%]) (Fig. 4C).

#### Pseudovirus infection assay in hiPSC-AEC rats

Pseudovirus infection assays were conducted on day 14 after the generation of hiPSC-AEC rats. The tracheae including the transplanted areas were collected on day 7 after infection (Fig. 5). The collected tracheae were subjected to immunohistochemistry analysis. The infected cells were identified by *GFP* expression and labeling by anti-*GFP* antibody to eliminate nonspecific stained cells. The infected hiPSC-derived cells, defined as *GFP*-positive, anti-*GFP* antibody labeling-positive, HNA-positive, and DAPI-positive cells, were observed in the tracheal submucosal layer of hiPSC-AEC rats (Fig. 6A, Supplemental Fig. S3A) and in the tracheal epithelia of two hiPSC-AEC rats (Fig. 6B, Supplemental Fig. S3B) in the virus infection group. The infected hiPSC-derived cells were mainly observed in the submucosal layer, and a small number of infected hiPSC-derived cells were also observed in the airway epithelium. The infected hiPSC-derived cells were not observed in the rats in the control group. The numbers of infected hiPSC-derived cells are shown in Table 2.

#### Discussion

In this study, we induced hiPSC-AECs, including multiciliated cells with motile cilia, which can become the first target cells of SARS-CoV-2 as in previous reports, prepared grafts by covering the artificial trachea with the hiPSC-AEC sheet and engrafted hiPSC-AECs in the tracheal epithelia to generate hiPSC-AEC rats. In the infection assay using these rats and pseudovirus, infected hiPSC-derived cells in all infected rats and an average of 10.5 infected hiPSC-derived cells per rat were identified. Infected hiPSC-derived cells were mainly located in the submucosal layer, and a small number of infected hiPSC-derived cells were also observed in the airway epithelia. To our knowledge, this is the first report of SARS-CoV-2 infection model using hiPSC-AEC rats.

In the infection assay using hACE2-mCherry/HEK293T cells, pseudovirus infection was indicated to rely on ACE2. In addition, in the infection assay using hiPSC-AECs, pseudovirus infection was confirmed. However, in the infection assay using pseudoviruses at a concentration of  $1 \times 10^7$  TU/mL, the infection rate in hACE2-mCherry/HEK293T cell was  $7.31\% \pm 1.75\%$ , whereas in the infection assay using pseudoviruses at a concentration of  $5 \times 10^8$  TU/mL, the infection rate in hiPSC-AECs was  $0.78\% \pm 0.45\%$ . We used lentiviral SARS-CoV-2 pseudoviruses containing SARS-CoV-2 S proteins and the *GFP* gene for infection assay. This pseudovirus cannot replicate in the host cells; therefore, it is less infectious than SARS-CoV-2.<sup>29</sup> In the future, infection assays using our

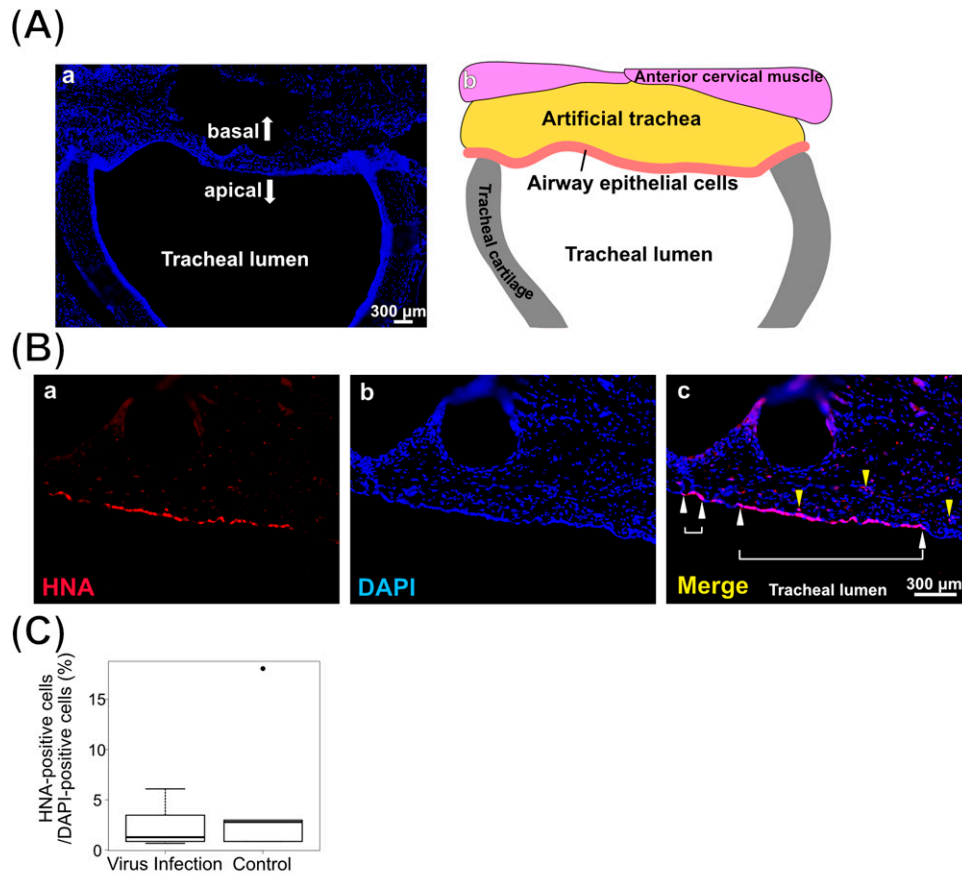


**FIG. 4.** Engraftment of hiPSC-AECs in the trachea after pseudovirus infection. (A) Vertical section of hiPSC-AEC rats after infection (a). Scale bars = 300  $\mu$ m. Scheme of the vertical section of hiPSC-AEC rats after infection (b). (B) Representative images of the immunofluorescence staining of engrafted hiPSC-AECs. HNA-positive engrafted cells (b) were observed in the transplanted area of the trachea (a). White arrowheads and white brackets show hiPSC-derived cells engrafted in the airway epithelium. Yellow arrowheads show hiPSC-derived cells engrafted in the submucosal layer (c). Scale bars = 300  $\mu$ m. (C) Comparison of the proportion of the survival cells in the total cells of the transplanted area in the virus infection and control groups. No statistical significance was observed. (Mann-Whitney  $U$  test, pseudovirus-infected rats,  $n = 6$ ; control rats,  $n = 5$ ). HNA, human nuclei antigen.

hiPSC-AEC rats and SARS-CoV-2 could increase the infection efficiency.

In the transplanted area in hiPSC-AEC rats after the infection assay, infected hiPSC-derived cells were mainly observed in the submucosal layer; on the contrary, only a small number of infected hiPSC-derived cells were observed in the airway epithelium. We performed infection assays 2 weeks after the

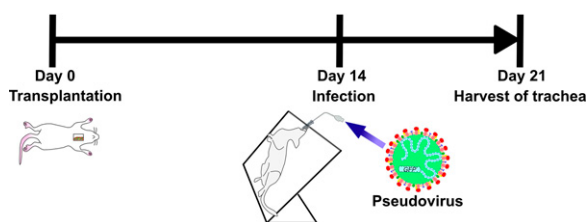


**FIG. 5.** Infection assay in hiPSC-AEC rats. Time course from the generation of hiPSC-AEC rats to the harvest of samples after infection. Infection experiments were performed on day 14 after the generation of hiPSC-AEC rats, and tracheal samples were harvested on day 7 after the infection (day 21 after the generation of hiPSC-AEC rats).

transplantation. At this point, transplanted cells formed cell-cell interactions with the recipient tissue based on our previous histological analysis.<sup>24</sup> However, tight junction barrier formation occurred after the localization of tight junction molecules.<sup>30</sup> From this, the sprayed pseudoviruses may have passed through the intercellular space, reached the submucosal layer, and been infected with cells in the submucosal layer. In the epithelial layer, surviving hiPSC-AECs were observed with sheet-like clusters in the recipient tracheae. As mentioned earlier, hiPSC-AECs contain various types of cells that constitute AECs.<sup>27</sup> In our model, various types of human-derived cells survived as sheet-like clusters in the transplanted areas; therefore, they can be used to examine the cell-cell interactions of target cells in SARS-CoV-2 infection as in the primary culture of bronchial cells.

Our animal model includes human cells. Respiratory infections are caused by various bacteria and viruses such as *Bordetella pertussis*<sup>31</sup> and human metapneumoviruses,<sup>32</sup> which strictly select human cells as hosts. The animal model generated in this study could be useful not only against SARS-CoV-2 but also against other human-specific infectious diseases. Our animal model is generated from nude rats

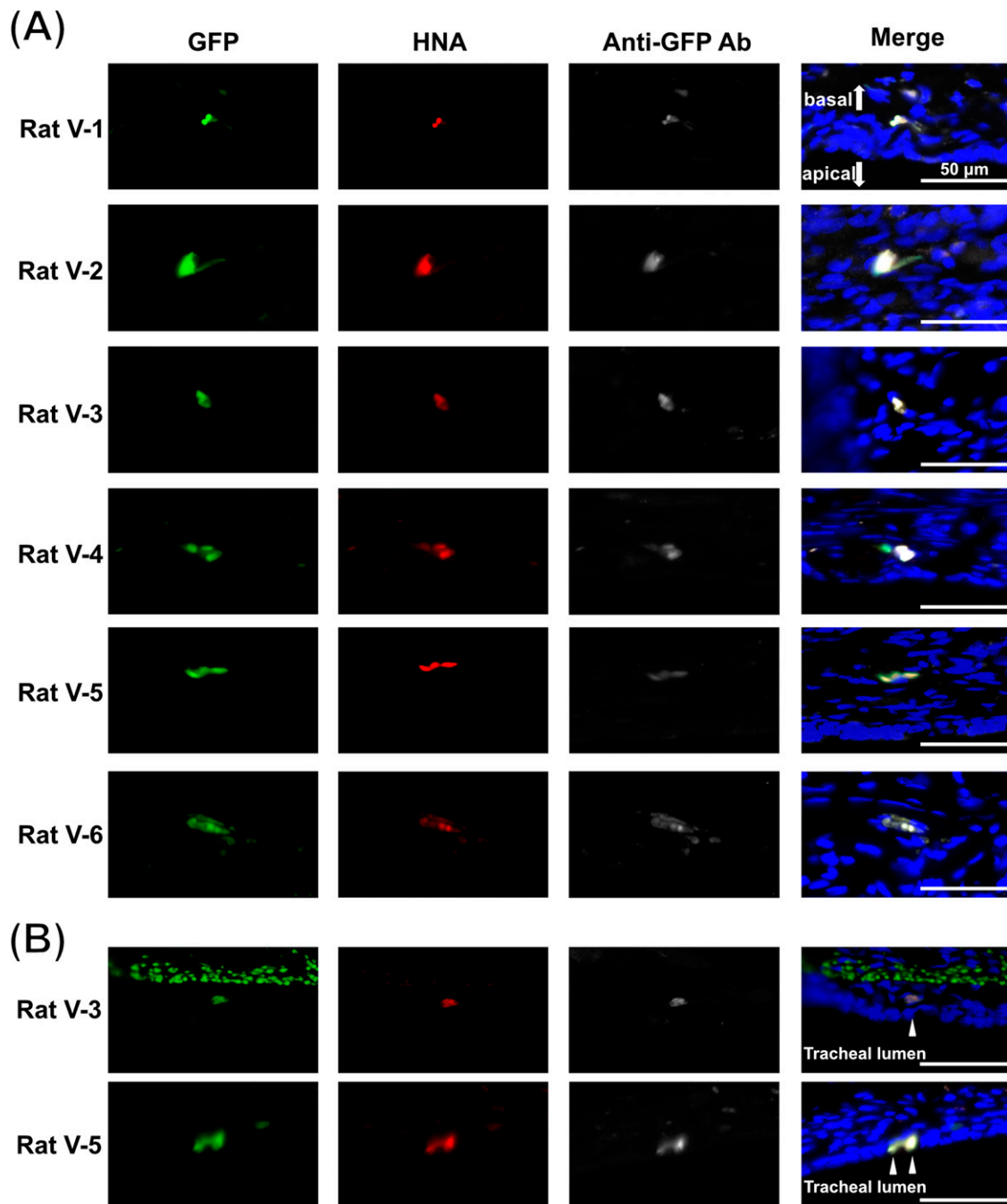


**FIG. 6.** Immunofluorescence staining images of tracheal samples after the infection assay. GFP, HNA, DAPI triple-positive, and anti-GFP antibody-labeled cells were defined as infected hiPSC-derived cells. Images of infected hiPSC-derived cells in the hiPSC-AEC rats of the infection group are shown. (A) Infected cells in the submucosal layer. (B) Infected cells in the airway epithelia. Scale bars = 50  $\mu\text{m}$ .

so far. It is considered that the use of more severe immunodeficient rats may generate trachea and immune system double-humanized rats in the future.<sup>33–35</sup> These double-humanized rats may contribute to future research on immune responses to respiratory infectious diseases.

As limitations, the infection efficiency of hiPSC-derived cells in our animal model is insufficient to enable the analysis of virus–host interactions and therapeutic effects at present. The possible cause is the low engraftment efficiency of transplanted hiPSC-AECs (Table 1). To improve the

engraftment efficiency of hiPSC-AECs, modifications of the induction method, scaffold materials, and strains of recipient rats may be considered.<sup>36–39</sup> In addition, the use of pseudoviruses is a point for improvement. As we mentioned in the paragraph on the infection efficiency in the pseudovirus infection assay in hiPSC-AECs, nonreplicative pseudoviruses were used for the infection assay. After the initial infection by the sprayed pseudovirus, the number of infected cells does not increase. Therefore, the infection efficiency of the pseudovirus infection assay is

TABLE 2. NUMBER OF INFECTED CELLS IN EACH GROUP

Rat no.	Group	Number of all infected cells (in the airway epithelia)
V-1	Infection	9 (0)
V-2	Infection	15 (0)
V-3	Infection	5 (1)
V-4	Infection	8 (0)
V-5	Infection	17 (2)
V-6	Infection	9 (0)
C-1	Control	0
C-2	Control	0
C-3	Control	0
C-4	Control	0
C-5	Control	0

lower than that of the SARS-CoV-2 infection assay.<sup>29,40</sup> Using SARS-CoV-2 in infection assays could increase the infection efficiency.

We used pseudoviruses with Omicron-type S proteins. According to reports of clinical symptoms, SARS-CoV-2 Omicron variant infection is associated with a higher frequency of upper respiratory tract symptoms,<sup>41</sup> and the variant has higher transmissibility than other variants.<sup>42</sup> Based on these reports, we consider that infection efficiency of the cells in the upper respiratory tract is higher in Omicron than in other variants, and we used pseudovirus with Omicron S proteins. However, the affinity of Omicron S proteins to hACE2 is intermediate between that of wild-type and Delta S proteins from recent findings.<sup>43,44</sup> Although Omicron S proteins have lower affinity for hACE2 than Delta S proteins, a clinical report found that the transmissibility of Omicron is ~3.2-fold higher than that of Delta,<sup>42</sup> and this transmissibility depends on the high immune evasion ability of Omicron.<sup>43,45,46</sup> These characteristics of Omicron might explain the low infection efficiency in this experiment, and it will allow the improvement of the infection efficiency using different variant pseudoviruses in the future. If the infection efficiency is increased, then this model could be used to examine virus–host interactions and validate therapeutic methods.

In conclusion, we confirmed that hiPSC-AEC rats, transplanted with grafts consisting of artificial tracheae covered with hiPSC-AEC sheets into tracheal defects, were infected with SARS-CoV-2 pseudovirus by spraying through the airway. Our results provide a basis for the development of infection models for respiratory infections that exhibit host specificity for humans.

### Acknowledgments

Snager sequencing services and immunofluorescent microscopy using Keyence All-in-One Fluorescence Microscope BZ-X810 were performed at the Medical Research Support Center, Graduate School of Medicine, Kyoto University. Electron microscopy was supported by the Division of Electron Microscopic Study, Center for Anatomical Studies, Graduate School of Medicine, Kyoto University.

### Authors' Contributions

K.O. and H.O. conceived and designed experiments in the study. M.K., H.O., A.M., T.M., Y.H., and K.M. conducted

the experiments and analyzed the results. M.K. and H.O. wrote the main article text and all figures. S.K., Y.K., T.K., Y.K., N.Y., and K.T. provided critical advice. All authors reviewed the article.

### Author Disclosure Statement

The authors declare no competing interests.

### Funding Information

This work was supported by the Japan Society for the Promotion of Science KAKENHI (21K19567), Alumni otolaryngology fund from the Department of Otolaryngology Head and Neck Surgery, Graduate School of Medicine, Kyoto University, and Kyoto University Medical Student and Researcher Support-Fund (KMS-FUND).

### Supplementary Material

Supplementary Figure S1  
Supplementary Figure S2  
Supplementary Figure S3

### References

1. Khalil-Khan A, Khan MA. The impact of COVID-19 on primary care: A scoping review. *Cureus* 2023;15(1):e33241; doi: 10.7759/cureus.33241
2. Naseer S, Khalid S, Parveen S, et al. COVID-19 outbreak: Impact on global economy. *Front Public Health* 2022;10(1):1009393; doi: 10.3389/fpubh.2022.1009393
3. Zhu Z, Lian X, Su X, et al. From SARS and MERS to COVID-19: A brief summary and comparison of severe acute respiratory infections caused by three highly pathogenic human coronaviruses. *Respir Res* 2020;21(1):224; doi: 10.1186/s12931-020-01479-w
4. Gupta A, Marzook H, Ahmad F. Comorbidities and clinical complications associated with SARS-CoV-2 infection: An overview. *Clin Exp Med* 2022;23(2):313–331; doi: 10.1007/s10238-022-00821-4
5. Menni C, Valdes AM, Polidori L, et al. Symptom prevalence, duration, and risk of hospital admission in individuals infected with SARS-CoV-2 during periods of omicron and delta variant dominance: A Prospective Observational Study from the ZOE COVID Study. *Lancet* 2022;399(10335):1618–1624; doi: 10.1016/S0140-6736(22)00327-0
6. Lamers MM, Haagmans BL. SARS-CoV-2 pathogenesis. *Nat Rev Microbiol* 2022;20(5):270–284; doi: 10.1038/s41579-022-00713-0
7. Khan M, Yoo S-J, Clijsters M, et al. Visualizing in deceased COVID-19 patients how SARS-CoV-2 attacks the respiratory and olfactory mucosae but spares the olfactory bulb. *Cell* 2021;184(24):5932–5949.e15; doi: 10.1016/j.cell.2021.10.027
8. Ward IL, Bermingham C, Ayoubkhani D, et al. Risk of covid-19 related deaths for SARS-CoV-2 omicron (B.1.1.529) compared with delta (B.1.617.2): Retrospective cohort study. *Bmj* 2022;378:e070695; doi: 10.1136/bmj-2022-070695
9. Jackson CB, Farzan M, Chen B, et al. Mechanisms of SARS-CoV-2 entry into cells. *Nat Rev Mol Cell Biol* 2022;23(1):3–20; doi: 10.1038/s41580-021-00418-x
10. Tatara AM. Role of tissue engineering in COVID-19 and future viral outbreaks. *Tissue Eng Part A* 2020;26(9-10):468–474; doi: 10.1089/ten.tea.2020.0094

11. Blanco-Melo D, Nilsson-Payant BE, Liu W-C, et al. Imbalanced host response to SARS-CoV-2 drives development of COVID-19. *Cell* 2020;181(5):1036–1045.e9; doi: 10.1016/j.cell.2020.04.026
12. Yamamoto M, Kiso M, Sakai-Tagawa Y, et al. The anticoagulant nafamostat potentially inhibits SARS-CoV-2 S protein-mediated fusion in a cell fusion assay system and viral infection *in vitro* in a cell-type-dependent manner. *Viruses* 2020;12(6):629; doi: 10.3390/v12060629
13. Ogando NS, Dalebout TJ, Zevenhoven-Dobbe JC, et al. SARS-coronavirus-2 replication in Vero E6 cells: replication kinetics, rapid adaptation and cytopathology. *J Gen Virol* 2020;101(9):925–940; doi: 10.1099/jgv.0.001453
14. Zhao MM, Yang WL, Yang FY, et al. Cathepsin L plays a key role in SARS-CoV-2 infection in humans and humanized mice and is a promising target for new drug development. *Signal Transduct Target Ther* 2021;6(1):134; doi: 10.1038/s41392-021-00558-8
15. Milewska A, Kula-Pacurar A, Wadas J, et al. Replication of severe acute respiratory syndrome coronavirus 2 in human respiratory epithelium. *J Virol* 2020;94(15); doi: 10.1128/JVI.00957-20
16. Djidrovski I, Georgiou M, Hughes GL, et al. SARS-CoV-2 infects an upper airway model derived from induced pluripotent stem cells. *Stem Cells* 2021;39(10):1310–1321; doi: 10.1002/stem.3422
17. Fang K-Y, Cao W-C, Xie T-A, et al. Exploration and validation of related hub gene expression during SARS-CoV-2 infection of human bronchial organoids. *Hum Genomics* 2021;15(1):18; doi: 10.1186/s40246-021-00316-5
18. Sano E, Suzuki T, Hashimoto R, et al. Cell response analysis in SARS-CoV-2 infected bronchial organoids. *Commun Biol* 2022;5(1):516; doi: 10.1038/s42003-022-03499-2
19. Yin F, Zhang X, Wang L, et al. HiPSC-derived multi-organoids-on-chip system for safety assessment of antidepressant drugs. *Lab Chip* 2021;21(3):571–581; doi: 10.1039/d0lc00921k
20. Shou S, Liu M, Yang Y, et al. Animal models for COVID-19: Hamsters, mouse, ferret, mink, tree shrew, and non-human primates. *Front Microbiol* 2021;12(8):626553; doi: 10.3389/fmicb.2021.626553
21. Fan C, Wu Y, Rui X, et al. Animal models for COVID-19: Advances, gaps and perspectives. *Signal Transduct Target Ther* 2022;7(1):220; doi: 10.1038/s41392-022-01087-8
22. Fu W, Wang W, Yuan L, et al. A SCID mouse-human lung xenograft model of SARS-CoV-2 infection. *Theranostics* 2021;11(13):6607–6615; doi: 10.7150/thno.58321
23. Kenney DJ, O'Connell AK, Turcinovic J, et al. Humanized mice reveal a macrophage-enriched gene signature defining human lung tissue protection during SARS-CoV-2 infection. *Cell Rep* 2022;39(3):110714; doi: 10.1016/j.celrep.2022.110714
24. Okuyama H, Ohnishi H, Nakamura R, et al. Transplantation of multiciliated airway cells derived from human iPSC cells using an artificial tracheal patch into rat trachea. *J Tissue Eng Regen Med* 2019;13(6):1019–1030; doi: 10.1002/term.2849
25. Miyamoto T, Hosoba K, Ochiai H, et al. The microtubule-depolymerizing activity of a mitotic kinesin protein KIF2A drives primary cilia disassembly coupled with cell proliferation. *Cell Rep* 2015;10(5):664–673; doi: 10.1016/j.celrep.2015.01.003
26. Gotoh S, Ito I, Nagasaki T, et al. Generation of alveolar epithelial spheroids via isolated progenitor cells from human pluripotent stem cells. *Stem Cell Rep* 2014;3(3):394–403; doi: 10.1016/j.stemcr.2014.07.005
27. Konishi S, Gotoh S, Tateishi K, et al. Directed induction of functional multi-ciliated cells in proximal airway epithelial spheroids from human pluripotent stem cells. *Stem Cell Rep* 2016;6(1):18–25; doi: 10.1016/j.stemcr.2015.11.010
28. Kanda Y. Investigation of the freely available easy-to-use software 'EZ' for medical statistics. *Bone Marrow Transplant* 2013;48(3):452–458; doi: 10.1038/bmt.2012.244
29. Huang J, Hume AJ, Abo KM, et al. SARS-CoV-2 infection of pluripotent stem cell-derived human lung alveolar type 2 cells elicits a rapid epithelial-intrinsic inflammatory response. *Cell Stem Cell* 2020;27(6):962–973.e7; doi: 10.1016/j.stem.2020.09.013
30. Suzuki R, Katsuno T, Kishimoto Y, et al. Process of tight junction recovery in the injured vocal fold epithelium: Morphological and paracellular permeability analysis. *Laryngoscope* 2018;128(4):E150–E156; doi: 10.1002/lary.26959
31. Diavatopoulos DA, Cummings CA, Schouls LM, et al. *Bordetella pertussis*, the causative agent of whooping cough, evolved from a distinct, human-associated lineage of *B. bronchiseptica*. *PLoS Pathog* 2005;1(4):e45; doi: 10.1371/journal.ppat.0010045
32. Jesse ST, Ludlow M, Osterhaus ADME. Zoonotic origins of human metapneumovirus: A journey from birds to humans. *Viruses* 2022;14(4):677; doi: 10.3390/v14040677
33. Yang X, Zhou J, He J, et al. An immune system-modified rat model for human stem cell transplantation research. *Stem Cell Rep* 2018;11(2):514–521; doi: 10.1016/j.stemcr.2018.06.004
34. Agarwal Y, Beatty C, Ho S, et al. Development of humanized mouse and rat models with full-thickness human skin and autologous immune cells. *Sci Rep* 2020;10(1):14598; doi: 10.1038/s41598-020-71548-z
35. Menoret S, Ouisse LH, Tesson L, et al. In vivo analysis of human immune responses in immunodeficient rats. *Transplantation* 2020;104(4):715–723; doi: 10.1097/TP.0000000000003047
36. Adigbli G, Menoret S, Cross AR, et al. Humanization of immunodeficient animals for the modeling of transplantation, graft versus host disease, and regenerative medicine. *Transplantation* 2020;104(11):2290–2306; doi: 10.1097/tp.0000000000003177
37. Hawkins FJ, Suzuki S, Beermann ML, et al. Derivation of airway basal stem cells from human pluripotent stem cells. *Cell Stem Cell* 2021;28(1):79–95.e8; doi: 10.1016/j.stem.2020.09.017
38. Rodrigues Toste De Carvalho AL, Liu H-Y, Chen Y-W, et al. The *in vitro* multilineage differentiation and maturation of lung and airway cells from human pluripotent stem cell-derived lung progenitors in 3D. *Nat Protoc* 2021;16(4):1802–1829; doi: 10.1038/s41596-020-00476-z
39. Varma R, Marin-Araujo AE, Rostami S, et al. Short-term preclinical application of functional human induced pluripotent stem cell-derived airway epithelial patches. *Adv Healthc Mater* 2021;10(21):e2100957; doi: 10.1002/adhm.202100957
40. Chen M, Zhang X-E. Construction and applications of SARS-CoV-2 pseudoviruses: A mini review. *Int J Biol Sci* 2021;17(6):1574–1580; doi: 10.7150/ijbs.59184
41. Akaishi T, Kushimoto S, Katori Y, et al. COVID-19-related symptoms during the SARS-CoV-2 omicron (B.1.1.529) variant surge in Japan. *Tohoku J Exp Med* 2022;258(2):103–110; doi: 10.1620/tjem.2022.j067

42. Long B, Carius BM, Chavez S, et al. Clinical update on COVID-19 for the emergency clinician: Presentation and evaluation. *Am J Emerg Med* 2022;54(4):46–57; doi: 10.1016/j.ajem.2022.01.028
43. Zhang X, Wu S, Wu B, et al. SARS-CoV-2 Omicron strain exhibits potent capabilities for immune evasion and viral entrance. *Signal Transduct Target Ther* 2021;6(1):430; doi: 10.1038/s41392-021-00852-5
44. Mannar D, Saville JW, Zhu X, et al. SARS-CoV-2 omicron variant: Antibody evasion and cryo-em structure of spike protein-ACE2 complex. *Science* 2022;375(6582):760–764; doi: 10.1126/science.abn7760
45. Dejnirattisai W, Shaw RH, Supasa P, et al. Com-COV2 study group. Reduced neutralisation of SARS-CoV-2 omicron B.1.1.529 variant by post-immunisation serum. *Lancet* 2022;399(10321):234–236; doi: 10.1016/s0140-6736(21)02844-0
46. Cameroni E, Bowen JE, Rosen LE, et al. Broadly neutralizing antibodies overcome SARS-CoV-2 Omicron antigenic shift. *Nature* 2022;602(7898):664–670; doi: 10.1038/s41586-021-04386-2

Address correspondence to:

*Koichi Omori, MD, PhD*

*Department of Otolaryngology-Head and Neck Surgery*

*Graduate School of Medicine*

*Kyoto University*

*54 Shogoin Kawahara-cho, Sakyo-ku, Kyoto City*

*Kyoto 606-8507*

*Japan*

*E-mail: omori@ent.kuhp.kyoto-u.ac.jp*

*Received: January 12, 2024*

*Accepted: May 15, 2024*

*Online Publication Date: June 27, 2024*